Temporal Variability in Seismic Maps of the Sun's Far Hemisphere and the Potential for Assessing Growth Rates of Active Regions

Charles Lindsey, NWRA

1. Introduction

The purpose of this analysis is to make a practical assessment of the potential of seismic maps of active regions in the Sun's far hemisphere for measuring the growth rates of said regions. It is well established that seismic maps of the Sun's far hemisphere show us the signatures of large active regions therein with a high reliability. In 2014, a year typical of a relatively weak solar maximum, the "Large Active Region Discriminator" of the Stanford "Far-Side Seismic Solar Monitor (FSSSM)" catalogued 141 signatures it attributed to "large active regions." Statistics on 22 counterparts of these signatures in February–May of 2011 (Interval 1) and January–April of 2012 (Interval 2) confirmed all of those as reliable identifications of real active regions, in terms of conspicuous excesses in both EUV emissivity and unsigned magnetic flux. Based upon these, we estimate the reliability of any given seismic signature recognized by the FSSSM Large Active Region Discriminator positively and accurately signifying an active region in terms of EUV emissivity and/or magnetic flux in conspicuous exess of the quiet Sun to be of order 97.5±2.5% for signatures that appear in the Sun's active-region bands.

Two basic questions now emerge:

1. With what accuracy can seismic signatures be used to assess various attributes of the active regions they signify in quantative terms, e.g., excess EUV emissivity, for irradiance forecasting, and excess unsigned magnetic flux, for implications respecting coronal magnetic fields, coronal hole locations in the far hemisphere, forecasting of high-speed streams, and projections of flare potentiality?
2. With what accuracy can seismic signatures project the growth rates of newly emerged magnetic flux in the Sun's far hemisphere, from the time of its first reconition to when it will rotate into direct view from earth, and from thence, during its subsequent transit across the near hemisphere?

The first point is addressed by comparing seismic signatures directly with the qualities concerned, excess EUV emissivity, excess unsigned magnetic flux, etc. For this re refer to the *Second Interim Progress Report* on *Monitoring Active Region Development on the Far Side of the Sun* for NOAA Project WC 133R-15-CN-0076 (`http://cora.nwra.com/~lindsey/NOAA_FarSide/Second_Report.pdf`). The point of this analysis will point 2, above: How well can seismic signatures in the far hemisphere quantitatively project properties of an active region to its appearance in the near hemisphere. Among the different aspects that can attach to this question are the following two:

(i.) the relationship between the growths of seismic signatures and the growths of properties mentioned above, and

(ii.) the accuracy with which the growth rates of the seismic signatures themselves can be measured.

Once again, the first point is addressed by comparing seismic signatures directly with the qualities concerned, for which we refer again to the Second Interim Report, cited above. The second concerns the behavior of the seismic signatures themselves with no concern for the qualities of active regions to which they are related. This is the object of this analysis.

The most fundamental limitation to the accuracy with which the strengths of seismic signatures can be measured is random noise. Helioseismic observations from SDO/HMI and GONG are now of such a quality that, for the special purposes of seismic monitoring of the Sun, instrumental noise is not a significant limitation. The major limitation is "realization noise." This can be regarded as noise due to truncation of the seismic observations to deliver the finite time-series that fit within the practical capacities of actual data analysis, particularly if temporal discrimination of conditions that are subject to change is to be preserved.[†]

Seismic maps of the Sun's far hemisphere, then, are invariably infected with noise irrespective of how clean the observations and how low the level of solar activity. Figure 1 shows an example of two composite seismic (far-side, amber) and line-of-sight magnetic (near-side, blue-gray) maps of the Sun published by the FSSSM in the early-rise phase of cycle 24. The amber portions are maps of the phase shift, $\Delta\phi$, between seismic oscillations that represent waves impinging from the near hemisphere into the locations represented as pixels in the far hemispehere and seismic oscillations, also in the near hemisphere, that represent the returning echos from the same. The phase shifts are expressed here in terms of travel-time perturbations, τ, in seconds. The travel-time-perturbation maps are integrated over 120 hours, the last 24 hours of which are centered on the dates posted at the tops of the respective frames, i.e., 2011-01-25.0 for the top frame and 2011-02-07.5 for the bottom. The bottom frame shows the signature of an active region at (340W,25N), which had been NOAA AR 11147 in its previous transit of the near hemisphere (and, as it had essentially died, NOAA left undesignated in its subsequent transit).

The bottom frame of Figure 1 also shows an extensive region, $\sim 20^\circ$ in radius centered at (050W,10S) in the near hemisphere (blue-gray) in which there was little magnetic

[†] A standard example of realization noise is in the practical determination of power spectra of filtered random noise. We understand that the power spectrum of a discrete time series of independently generated Gaussian random values is statistically flat. However, when we compute the discrete Fourier transform of such a time series and plot the square of its modulus, the result is invariably a spectrum that is far from flat, one that is fully as stochastic in frequency as the square of the original time series is in time. What is flat is the mean of an infinite ensemble of such power spectra, independently produced. Realization noise refers to the difference between the mean power spectrum averaged over a finite ensemble and the ideal case of an infinite ensemble—whether the resulting spectrum is flat or otherwise. Optical imaging both in seismic and electromagnetic spectra is subject to realization noise in ways highly analogous to those well known to apply to power spectra.

flux on 2011-02-07.5. The top frame shows the same region when it was in the far hemisphere, 13.5 days before. The rms seismic signature, $\Delta\phi$, over this relatively quiet region in the 2011-01-25.0 map is 0.02 radian, i.e., corresponding to an rms travel-time perturbation, $\Delta\tau$, of 1.0 sec in travel time, $\Delta\tau$. We take this to be the basic noise limit for a single spatial-resolution element, whose dimension is set by diffraction to 10° on the Sun's surface.

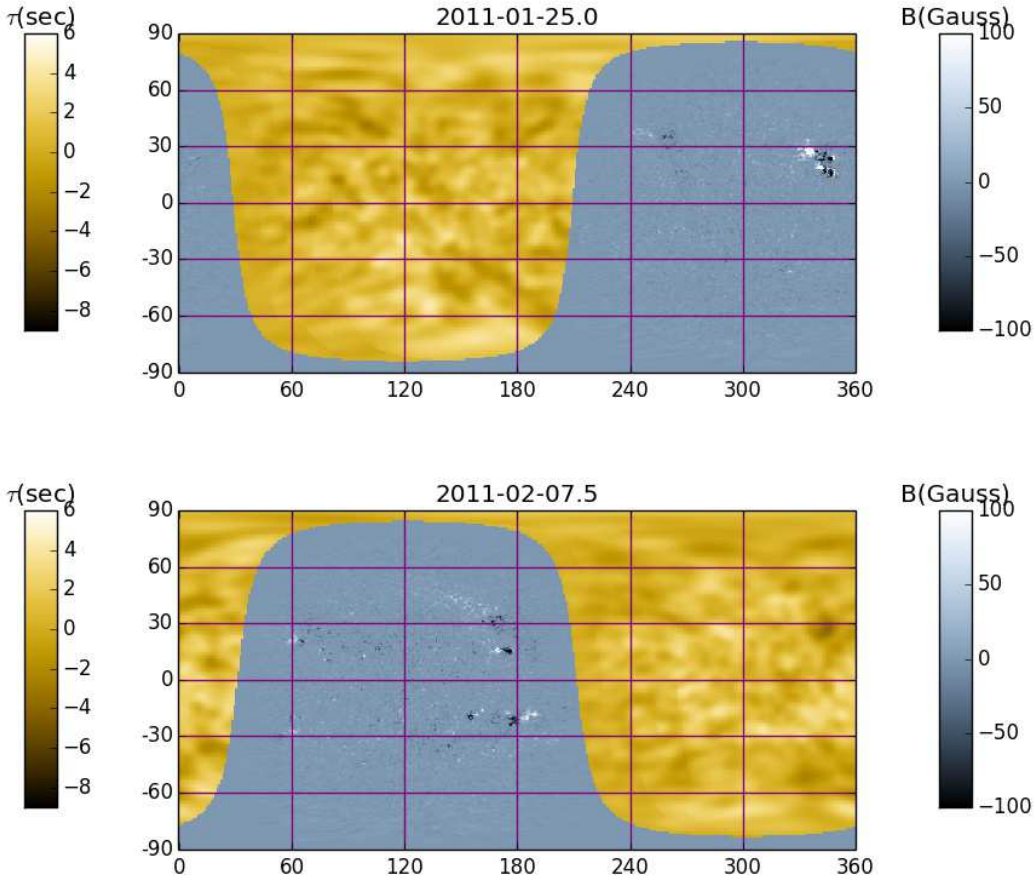

Figure 1. Seismic maps of the Sun's far hemisphere (amber) in early 2011, in the early-rise phase of cycle 24. Large regions on the Sun were free of conspicuous excesses of magnetic flux.

2. The Database

We have already introduced the seismic maps published by the Stanford FSSSM, showing samples in Figure 1. The basic data product computed by the FSSSM is a map of the far hemisphere representing seismic correlations between waves converging to focal points in the far hemisphere and their returning echos integrated over 24-hour periods. These "24-hour snapshots," are produced at 12-hour intervals. The most useful data product for a broad range of applications is 5-day (120-hr) means of the 24-hour snap-

shots, for a signal-to-noise that is greatly improved over that of the 24-hour snapshots, even if at some possible expense in temporal resolution.*

For the analysis that follows, we define the "strength," S, of a seismic signature by

$$S(\mathcal{R}) \;=\; \frac{1}{2\pi}\int_{\mathcal{R}} \Delta\phi \; d^2a, \tag{1}$$

the integral being taken over some region $\mathcal{R}$ that encompasses the signature. The random variation in S that attaches to a given seismic signature depends on the area, A, over which the seismic signature is distributed. An analysis is possible that considers both S and A. However, the present analysis will be based simply on the statistical variation in S, as catalogued by the FSSSM Large Active Region Discriminator. This conflates, to some extent, noise in the diagnostic with variations in the behavior of active regions themselves that appear to be resistant to long-term forecasting, i.e., stochastic variations occurring in the active regions on short time scales.

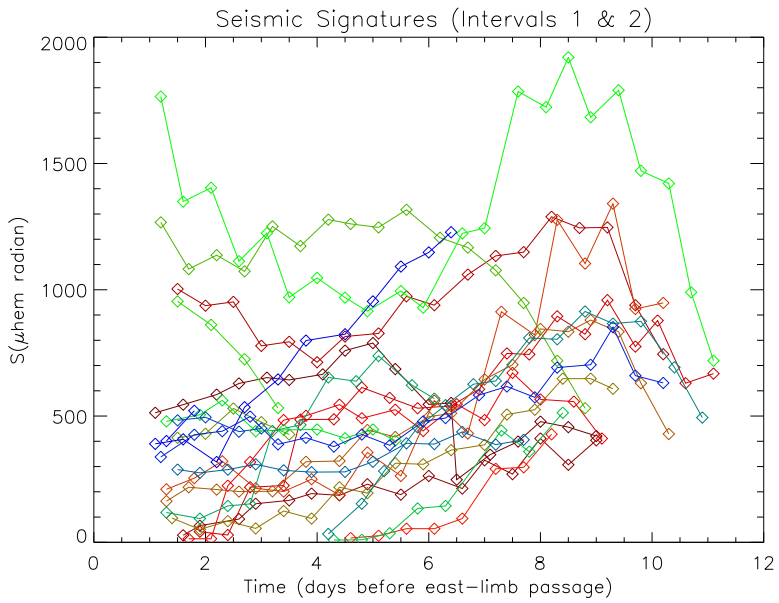

Figure 2. Seismic profiles, S, of the 22 seismic signatures of the active regions in Intervals 1 and 2 of this study. Time is represented in days *before* east-limb passage. Hence, time proceeds from the right of the plot to the left, the east-limb passage being at the left ordinate axis. The profile of the first seismic signature, that of FS-2011-002, first appearing in the far hemisphere on 2011-02-15 and rotating into the near hemisphere on 2011-02-25, is plotted in magenta. Plots of subsequently appearing signatures are colored in the order of the colors of the rainbow, ending with FS-2012-010 (2012-04-08 to 2012-04-10) in bright blue.

* For purposes of gauging growth rates, any loss of temporal discrimination resulting from averaging multiple maps together for each day in place of a single snapshot is only apparent. The way the 5-day means are computed is invertible; thus, the 24-hour snapshots can be reconstucted from the 5-day means with all of the original information on growth rates preserved.

Figure 2 shows plots of the the strengths, S, of all of the 22 FSSSM large-active-region seismic signatures in Intervals 1 and 2 during the last up to 11 days of their respective transits of the far hemisphere. This dataset is posted on `http://cora.nwra.com/~lindsey/NOAA_FarSide/Seismic_Sigs.txt`. Figure 2 plots the strengths, S, as a function of time *before* the active region befor a given signature arrives at the Sun's eastern limb, with arrival thereat referenced to the left ordinate axis. Hence, the active regions can be considered to be moving in time from the right of the plot domain to the left. These time series are truncated at approximately 36 hours before passage across the east limb (left edge of Figure), where partial disappearance of the signature from the seismic map as it rotates into the near hemisphere would otherwise cause an artificial decline in the seismic signature.

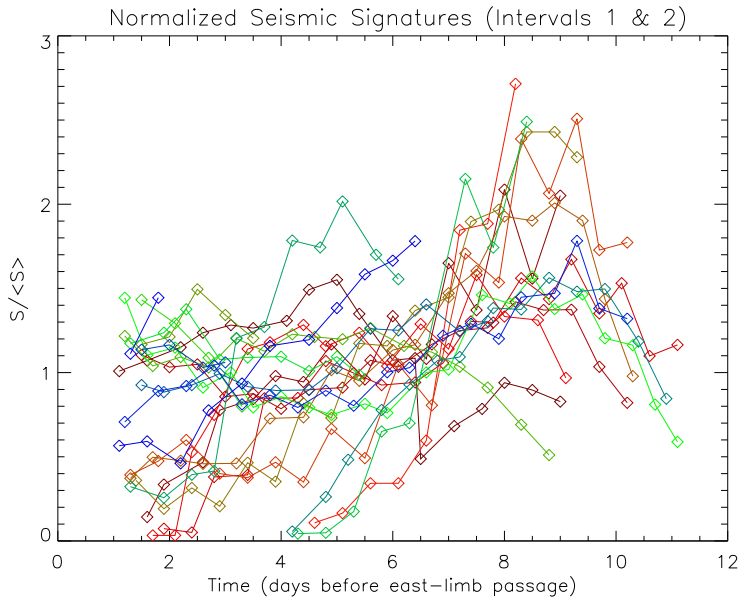

Figure 3. Same as Figure 2, but, each profile is normalized to a mean value of unity.

There is a general tendency for all of the signatures plotted to appear relatively precipitously, and thence to decay, usually somewhat more gradually. This may be more easily seen Figure 3, in which all of the plots have been normalized to a mean of unity. This shows that the precipitous rise can be up to a factor of two from the signature's initial recognition by the FSSSM Large Active Region Discriminator to the succeeding peak. This tendency of precipitous rise followed by a slower, roughly monotonic decay strongly reflects both their EUV-intensity and magnetic-flux counterparts (Ugarte-Urra et al. 2015). The further succeeding decay, though generally slower, can still exceed an order of magnitude, the signature all but disappearing before its location rotates into view from Earth. There are, nevertheless, major and frequent exceptions to this tendency, i.e., active regions that undergo persistent growth for up to a week, and others whose decays are interrupted by a precipitous growth spurts.

3. The Model

We now turn to the question of what parts of the variations shown by the seismic profiles plotted in Figure 1 represent actual variations in the active regions that elicit the seismic signatures, and what can more plausibly be regarded as noise, whether the result of "realization" (see discussion in §2.1), spurious instrumental contributions, or just unpredictable qualities of the active regions that give ise to seismic signatures. It is quite evident, from seismic maps of the Sun's far hemisphere when there is a minimum of solar activity, that the diagnostic is noisy, $\Delta\phi$ showing variations of order 0.02 radian all over the far hemisphere with no apparent relation to any features that have any relationship to the Sun or the solar environment. But, real stochastic qualities in the evolution of active regions can introduce qualities that are similarly noise like from the practical vantage of forecasting in what condition said active region will be in the future—even when the diagnostic represents the present condition faithfully. What follows, then, is an effort to discriminate some of the noise-like, qualities in the signatures catalogued by the FSSSM from those that are more "trendy," hence more amenable to forecasts.

For a considerable class of noisy phenomena, the following general dynamical model can be adapted to represent the reality with some degree of approximation. We will proceed with this as a hypothetical starting point: This model conveniently applies when the signatures, S, we can avail consist of a temporally ordered set of samples, $(S_1, S_2, ..., S_n)$, delivered at regular intervals. We suppose that

$$S_i \;=\; R_i \;+\; N_i, \tag{2}$$

where N_i represents random stationary Gaussian, i.e., "white," noise in which

$$\begin{aligned} \langle N_i \rangle \;&\equiv\; \frac{1}{N}\sum_{i=1}^{n} N_i \;=\; 0, \\ \langle N_i N_j \rangle \;&=\; N_0^2\;\delta_{ij} \text{ and} \\ \langle N_i R_j \rangle \;&=\; 0 \\ \forall\; i,\; j \;&\in\; \{1, 2, ..., n\}. \end{aligned} \tag{3}$$

Furthermore, we suppose that R_i is non-negative, in accordance with the seismic signatures of the FSSSM being all positive, but devolving to zero in the absence of activity—as a proxy for the non-existence of a recognized signature, S, when or where that shown by the seismic map falls below the positive threshold of the FSSSM Large Active Region discriminator.

Now, when the focus is on the discrimination and assessment of the noise part, N, of S from R, based on the characters described by equations (3), and the imposition that $R \geq 0$, there are strong advantages to looking at the *differences*,

$$\Delta_i S \;\equiv\; S_i \;-\; S_{i-1}\;\forall\; i \;\in\; \{2, 3, ..., n\} \tag{4}$$

between *consecutive samples* of S. Figure (4) plots these against the intermediate values,

$$S_{mi} \;=\; \frac{1}{2}(S_i \;+\; S_{i-1}), \tag{5}$$

between S_i and S_{i-1}.

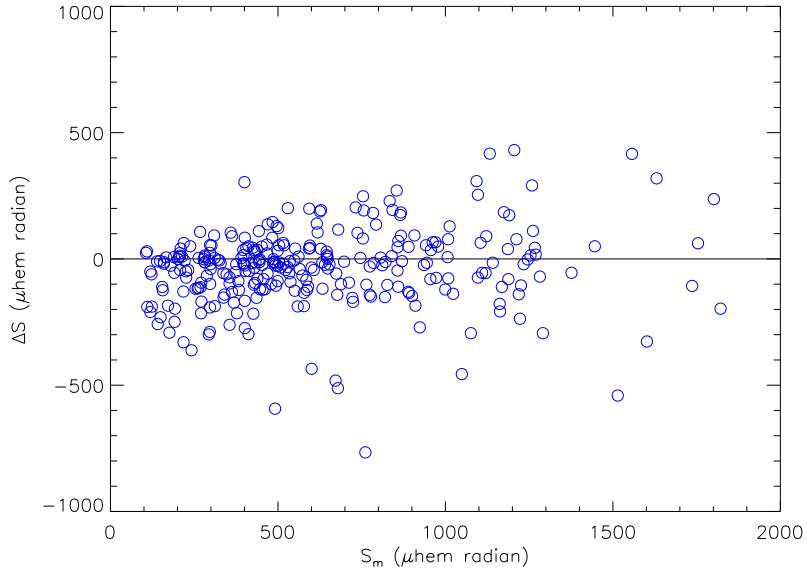

Figure 4. Consecutive (12-hr) sample variations, ΔS, in the strength, S, of the seismic signature (ordinate) are plotted against S_m itself (abscissa) for the FSSSM large-active-region signatures in Intervals 1 and 2.

This plot shows a dense clustering of points roughly along the abscissa axis for seismic signatures whose strengths are less than about 700 μhem radian. The crowding toward the left center is partly because there are more relatively weak signatures than strong ones. Moreover, the distribution of the weaker signatures plotted leftwardly is more compact in ordinate range. Weaker signatures vary less than stronger ones. Finally, where $S_m < 500$ μhem radian, there are significantly more negative consecutive differences than positive ones. As evident in Figure 1, more signatures are decreasing as time progresses (to the left in Figure 2) than increasing.

For a statistical assessment of the general dependence of the root mean square deviations of $\Delta_{\rm rms}S$, of S_i from S_m, we partition the abscissa domain into 100-μhem-radian segments, compile the means of ΔS^2 for all of the data points whose value of S_m lie in each range, take the square roots of all of these, and plot them. Figure 5 shows the result: Because of the sparsity of data points with S_m exceeding 1,200 μhem-radian, the partition interval for these is expanded from 100 μhem-radian to 200.

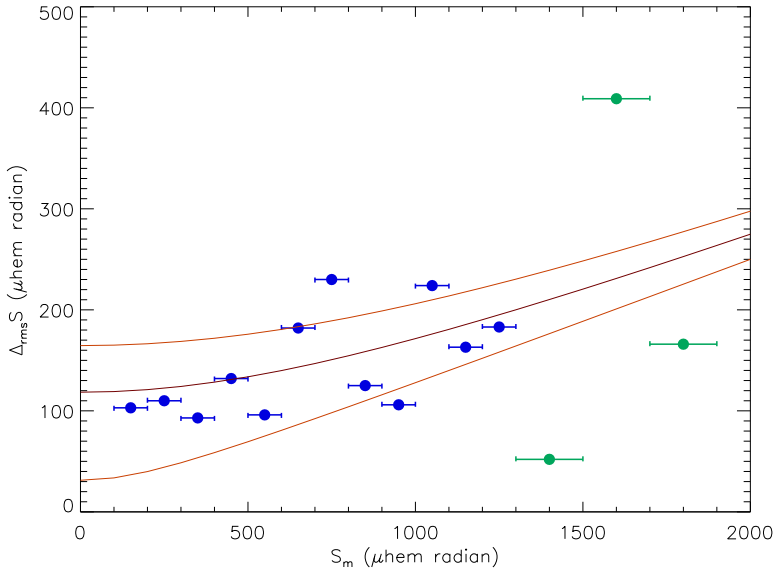

Figure 5. The rms consecutive-sample variation $\Delta S_{\rm rms}$, in the strength, S, of the seismic signatures plotted in Figure 2 are plotted here as a function of S_m. The rms variation, $\Delta_{\rm rms}S$, appears to be a slowly increasing function of S_m. The strength ranges that contain ten or more samples are plotted in blue. The total number of samples in the entire range of strengths above 1,200 is only nine. These statistically weaker varations are plotted in green. The magenta-colored line shows the best linear fit to the statistically strong (blue) variations, with orange lines marking the rms deviation of the blue data points above and below the fit.

Under the conditions stated by equations (3), the mean squares, $\Delta^2 S$ and $\Delta^2 R$, of ΔS (ordinate in Figure 4) and ΔR, respectively, are related by

$$\langle \Delta^2 S \rangle \;=\; 2N_0^2 \;+\; \langle \Delta^2 R \rangle \;=\; 2\big(N_0^2 \;+\; \langle R^2 \rangle\big). \tag{6}$$

The magenta colored curve in Figure 5 represents the best fit of the blue data points to the function

$$\langle \Delta^2 S \rangle \;=\; 2N_0^2 \;+\; \frac{1}{2}\kappa \langle R \rangle^2 \;+\; O\langle R \rangle^4. \tag{7}$$

The resulting fit parameters are

$$\begin{aligned} 2N_0^2 \;&=\; (118\ \mu\text{hem radian})^2,\ \text{hence},\ N_0 \;=\; (84\ \mu\text{hem radian}),\ \text{and} \\ \kappa \;&=\; 0.0308. \end{aligned} \tag{8}$$

We consider the exercise of estimating the growth rate of a seismic strength, S, over a five-day period by the simple approach of making two measurements of S five days apart, and taking the derivative to be the difference between them divided by five days. The error in the difference should be $\sqrt{2}N_0$. If we extrapolate the derivative five days into the future of the second of the two measurements, then the uncertainty attached to the extrapolation is $\sqrt{2}N_0$. But, the second measurement also has an uncertainty, of

N_0. Combining the second uncertainty in quadrature with the first leads to a composite uncertainty of

$$\Delta S(+5 \text{ days}) \;=\; \sqrt{3} N_0 = 145 \; \mu\text{hem radian}. \tag{9}$$

3. Conclusions

As Figures 2 and 3 show, active-region seismic signatures typically change by a factor of two over five days. So, for an active region whose seismic strength reaches something like 500 μhem radian at some point, a five-day projection based on a five-day difference ought to discriminate a rapidly growing region from a typically decaying one with several times the basic uncertainty of 145 μhem radian we estimate for the nominal 5-day projection. For growth projections attempted over shorter periods, Δt, we understand the error that applies to be in proportion to $\Delta t^{-3/2}$. This is because (1) the denominator by which the difference in the measurements of S is directly proportional to Δt, and (2) the accuracy of the measurements of S are proportional to $\Delta t^{-1/2}$ (since the number of independent samples is in direct proportion to Δt and the accuracy of the mean is in proportion to the square root of the number of independent samples).

The foregoing projections assume that growth rates, once they are measured will be maintained. Realistic active regions can change from rapidly growing to decaying in a five-day period (Ugarte-Urra et al. 2015). Hence, for most active regions that break the FSSSM large-active-region threshold, the major consideration in extrapolating their growth rates based on 5 days of previous seismic signatures appears to be the predictability of their "actual behavior" as much as the accuracy of the diagnostic.

6. Reference

Ugarte-Urra, I., Warren, H. P. & Hathaway, D. H. 2015 "Magnetic Flux Transport and the Long-Term Evolution of Solar Actie Regions," *Ap. J.* **815**, 90.